Deep nulling of laser light in a rotational shearing interferometer

S.R. Martin, E. Serabyn, & G.J. Hardy
Jet Propulsion Laboratory
Mail Stop 301-451
4800 Oak Grove Drive
California Institute of Technology
Pasadena, CA 91109
818-354-5861
Stefan.R.Martin@jpl.nasa.gov

ABSTRACT

There is great interest in techniques that potentially enable the direct detection of light from planets orbiting nearby stars. In one technique, nulling interferometry[1,2,3,4], the light from two or more separate telescopes can be destructively interfered to cancel the light from the star, allowing detection of the faint off-axis light from an orbiting planet or circumstellar disc. At the Jet Propulsion Laboratory, broadband white light nulls limited by dispersion effects have been previously reported[1]. In this paper, we investigate other limiting effects using a monochromatic laser source. We report transient laser nulls as deep as 1 part in 10^6 and stabilized nulls as deep as 1 part in 10^5 at a wavelength of 633 nm and discuss the techniques used to obtain these nulls and the residual sources of stray light. We compare the measured performance of the rotational shearing interferometer with a theoretical model.

1. INTRODUCTION

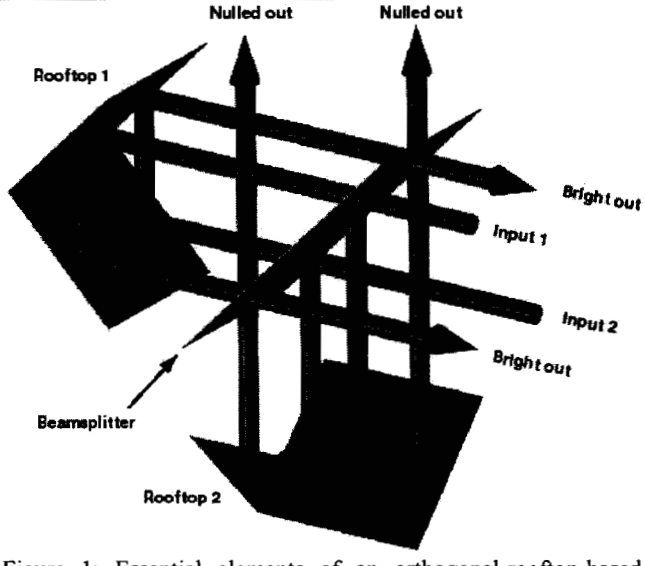

Figure 1: Essential elements of an orthogonal-rooftop-based rotational shearing interferometer. At zero optical path difference, the two input beams to be superposed yield two achromatically nulled output beams and two bright outputs.

In a nulling interferometer, the primary objective is to impose an achromatic 180 degree field flip on one of the two input beams and then combine the input beams to form a destructive interference at zero OPD over a broad waveband. For astronomy, this implies that light from an on-axis object will be extinguished (or rejected at the beamsplitter) and therefore faint, slightly off-axis objects, for example planets orbiting a star, might be detected. This field-flip can be achieved in a number of ways, for example using rooftop mirrors[6,7], dispersive elements[8], or extra foci[9]. One of the main challenges in the construction of a successful nulling interferometer is the high degree of symmetry required, so that each input beam experiences an equivalent optical path as it travels through the system.

In the rotational shearing interferometer, the input beams are split at a beamsplitter and the resulting output beams are propagated to rooftop mirrors arranged on orthogonal axes. The effect of the orthogonal rooftops is that one beam has its vertical polarization flipped by 180° and the other has its horizontal polarization flipped by 180°. The beams then return to the beamsplitter and are subtracted or nulled at one output; the other beamsplitter output in the direction of the input beams being the constructive output. Figure 1 shows the layout of the rooftop mirrors and the input and output beams.

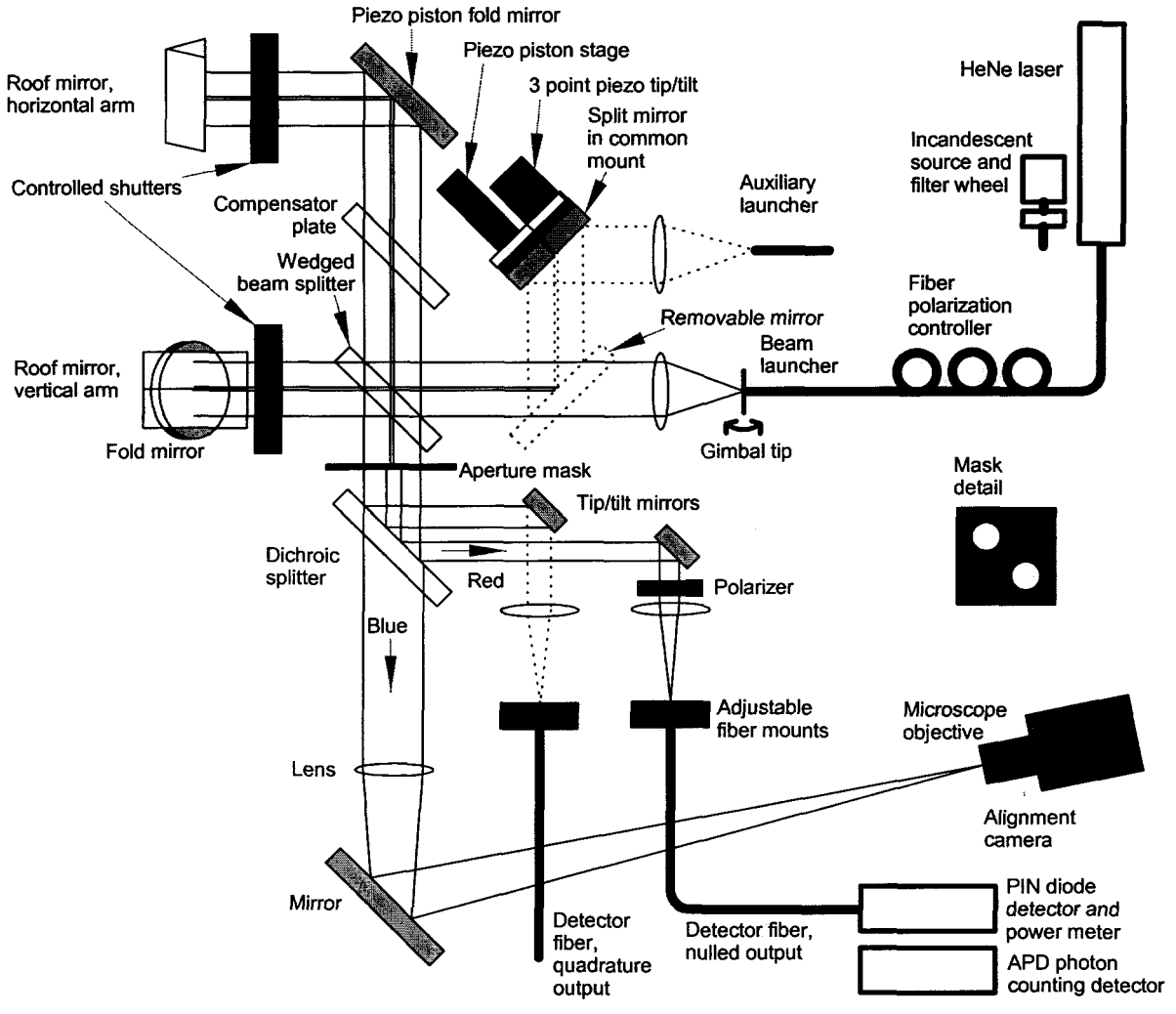

Figure 2: Layout of the nuller showing two setups. For the deep laser null experiments described here, the removable mirror was removed and the beam launcher supplied by either a HeNe laser or an incandescent source. Only one aperture of the mask was utilized, and only one of the detector outputs. (With the removable mirror in place, the nuller could be employed to test quadrature null stabilization approaches by introducing a phase shift on one of the input beams[10]).

In each path, a fold mirror is placed so as to produce equal numbers of s and p reflections for each polarization component present in the beam; Figure 2 shows the complete layout and Figure 3 a photograph of the equipment. A second effect of the rooftops is to shear the beams relative to the input, one beam being sheared vertically, the other horizontally. To obtain overlapping exit pupils, the input pupil must therefore be centered at the apparent crossing point of the two rooftop axes (seen through the beamsplitter) thus yielding zero shear, or alternatively, two identical input beams must be provided evenly centered on a 45° axis through the crossing point. This configuration is attractive for a separated spacecraft interferometer, while the other configuration could be operated with a single aperture nulling telescope (stray reflections from rooftop facets allowing). In the 45° configuration, the bright constructive fringe output of the beamsplitter is returned towards the input beam but sheared across the orthogonal diagonal.

2. BEAM INJECTION AND OUTPUT

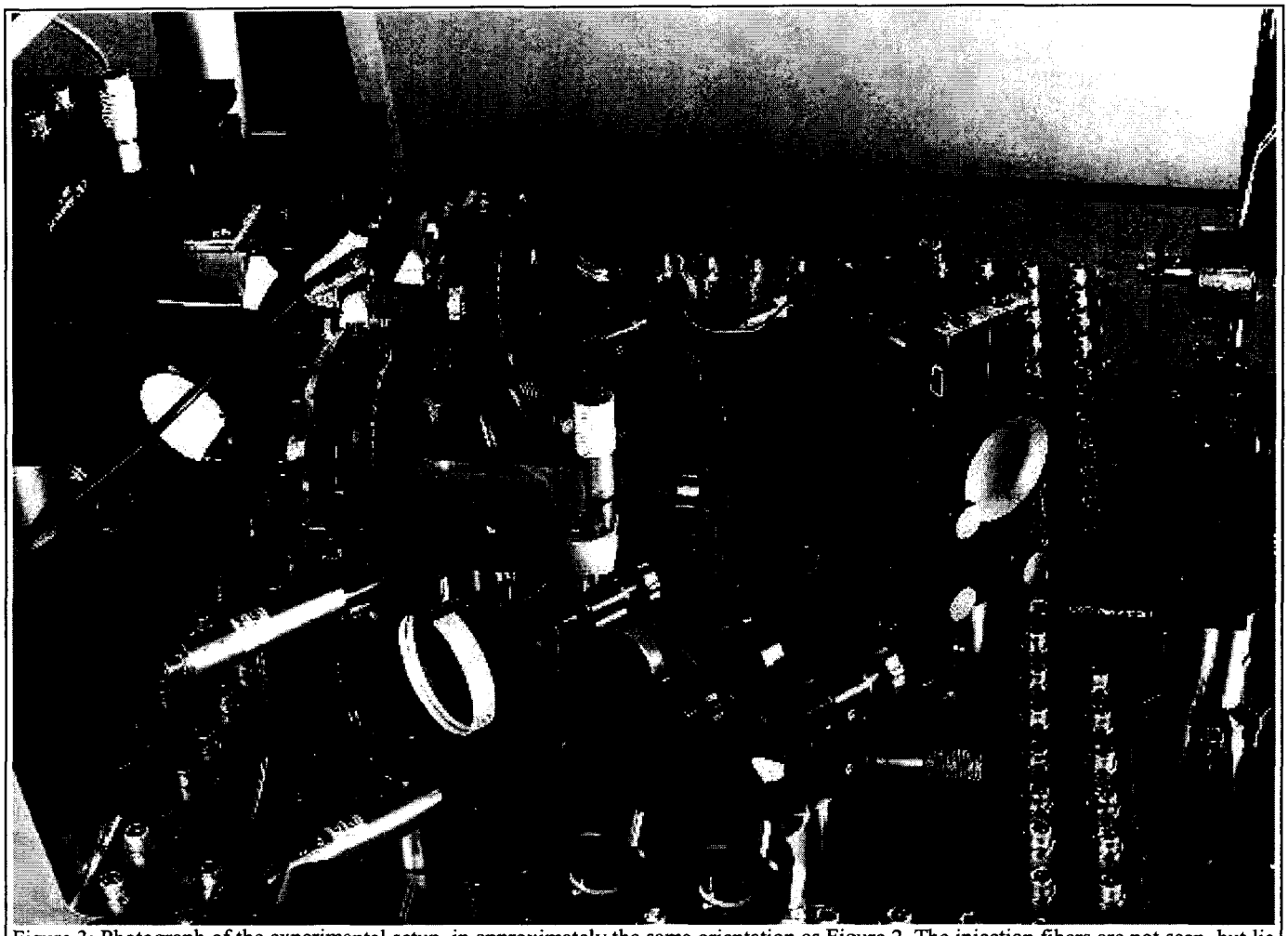

Figure 3: Photograph of the experimental setup, in approximately the same orientation as Figure 2. The injection fibers are not seen, but lie just off the right hand edge of the figure. The input lens mount is seen edge-on on the right, along with a shutter. The split mirror toward the top right and the back of the removable mirror just below it were not used in these experiments. The beamsplitter and compensator are located just left of center in the picture, and the two rooftop mirrors are seen toward the left. One 45° fold mirror is seen below the leftmost rooftop mirror, while the other is located top-center in the figure. The dichroic splitter (see Figure 2) is located at the bottom left. Finally, twin output beams are located at the bottom center of the picture, with two sets of fold mirrors, polarizers and lenses; but only one output was used for these experiments. The output fiber and the alignment camera are also out of the field of view.

Light was delivered to the nuller via a single mode fiber. The fiber provided a rapid means of changing the light source without requiring realignment of the nuller. The fiber launcher was also fitted with a polarizer and polarization control device to enable injection of a single polarization state, aligned with the beamsplitter and other surfaces. The fiber and its collimating lens also provided a clean, plane wavefront input to the nuller. Referring to Figure 2, two input points are provided, the upper one via a twin mirror arrangement was used for white light and dual output experiments. The lower input was used for laser experiments by removing a mirror.

At the exit of the nuller, a lens and a second single mode fiber was used to collect the light. The f number of the output was chosen to be larger than required to efficiently couple to the fiber, so that the fiber effectively sampled a small region of the central Airy disc, improving null depth by rejecting low spatial frequency wavefront aberrations.

3. POLARIZATION

The beamsplitter was used at 45° incidence angle; only one polarization was used because of apparent OPD dispersion for the s and p reflections. The source of this dispersion is unclear, since the nuller was designed to be symmetrical with respect to s and p polarizations. However, there are some remaining asymmetries in our design, most notably in the beamsplitter/compensator plate arrangement, so the s-p difference is probably attributable to this.

4. DISPERSION CONTROL

The beamsplitter was a single plate of glass with an antireflection (AR) coating on one surface and a dielectric 50/50 splitter coating on the other surface. Light transmitted through the beamsplitter and then reflected on its return would make three passes through the plate and encounter the beamsplitter in transmission then reflection ($BS_{T,R}$) and make three passes through the AR coating ($AR_{T,T,T}$). The beam initially reflected from the beamsplitter would make only one pass through the glass (on its return pass) so a compensator plate is introduced in the second arm of the interferometer. This second piece of glass is AR coated on both sides so the beam encounters $BS_{R,T}$ and $AR_{T,T,T,T,T}$. Therefore there is an asymmetry in the beam paths which could result in some dispersion of optical path between the two arms of the nuller. For a narrow band source such as a laser, this dispersion is negligible. When using this equipment for white light nulls, we were able to tune the dispersion by tilting the compensator plate slightly and achieve white light nulls of 70000 for 18% bandwidth input light. Ideally an 'immersed' beamsplitter could be used which would have the beamsplitter surface sandwiched between identical pieces of glass. However these splitters are comparatively difficult to make, because the plate thicknesses have to be carefully controlled, and there are tight bond line control or plate flatness requirements.

5. INTENSITY CONTROL

In these experiments, we employed a single aperture at the output of the beamsplitter, located on a 45° axis. Figure 2 shows a two aperture mask employed for dual output experiments; in this case we blocked one of the exit pupils. The single aperture avoided rooftop facet reflections and allowed control of the relative intensity of the two input beams. The input beam was fed to the system via a single mode fiber and allowed to expand before collimation by an achromatic lens. The fiber was mounted in a gimbal so that its optical axis could be angled with respect to the optical axis of the nuller. The single output pupil traced back through the system to the entrance forms two input apertures and by angling the fiber the relative intensity of the light entering each input could be accurately controlled. This control was important for deep nulling. To achieve an intensity match between the two input apertures an incandescent light source was used, filtered through a red bandpass filter set to a bandwidth of about 100 nm and detected using a photon counting module, integrating for several seconds. The incandescent source was very stable (<0.1% short term variation) compared to the laser (5% short term variation) and permitted accurate balancing of the intensity in the two nuller arms. To facilitate this balancing, the fiber input to the nuller could be connected to the laser source or to the incandescent source and the output fiber could be connected either to a PIN diode detector or to an avalanche photodiode photon counting module.

6. ALIGNMENT

Alignment was facilitated by a dichroic mirror which transmits blue light to a camera and video monitor, allowing angle sensing of the input beams. For laser experiments, the dichroic also transmits sufficient laser light to allow its use. Each arm of the nuller has a shutter which allows positioning of one beam at a time. Tilting of the rooftop mirror allowed alignment along one axis and since the rooftop axes are orthogonal, the beams could be brought to a common position. Fine tuning of the alignment would be done during the nulling experiment.

7. SOURCES OF NULL DEGRADATION

To obtain deep nulls, a number of parameters need to be carefully controlled. A high degree of symmetry[11] between the interfering beams is required: the electric field vectors of the two input beams must be oppositely oriented, the beams must have equal intensities, there must be zero relative path difference. For nulling of light from astronomical objects, we must also achieve a simultaneous zero of OPD for both polarizations and cancellation at all wavelengths in the passband. To these optical requirements we must also add alignment requirements such as very small angular tilt between the beams and almost exact overlap (zero shear) of the input apertures. In addition, there are opto-mechanical

requirements such as very small wavefront differences between the beams. These wavefront differences might arise from optical surface profile variations or from diffraction within the optical system.

The null depth N is defined as the ratio of the intensity of leakage through the null divided by the intensity at the peak constructive interference. N depends on a number of factors which need to be carefully controlled. For high fringe visibility V, the null depth N is equal to (1-V)/(1+V) ~ (1-V)/2. The overall null depth achievable in the system is the algebraic sum of the individual contributions to the null, so it makes sense to reduce the number of parameters contributing to the null degradation. Table 1 shows some parameters which contribute to the null and shows their relationships to the null depth making the assumption that the null is deep and the deviation of the parameter from zero is small. All the listed parameters (except for stray light) contribute linearly to the square root of the null.

The beamsplitter and compensator plate are sources of secondary reflections which will reduce the null depth. These components were therefore slightly wedged at 34 arc sec and the wedges were aligned in orthogonal directions to avoid superimposing stray reflections on the focal plane. The effect of the wedge is to throw stray light traveling in the direction of the transmitted beam 56 arc secs away from the direction of the main beam.

There are three major contributors to the secondary reflections: two paths for light passing through the beamsplitter coating initially and one path for light initially reflected from the beamsplitter. In the nomenclature used earlier, these paths are $BS_TAR_RBS_RAR_{T,T}BS_RAR_T$, $BS_TAR_{T,T}BS_RAR_RBS_RAR_T$, and $BS_RAR_{T,T,T,T}BS_TAR_RBS_RAR_T$. These three paths contribute 0.066% of the light at the focal plane. Other paths involving the compensator plate are neglected since they would require two reflections from the AR surface. The secondary beams are slightly displaced from the center of the focal plane by the wedging and taking into account the Airy profile of the focal spots, would be expected to produce a best case null depth of $4.6\ 10^{-7}$. This estimate is based on incoherent addition of the light. In fact, there would be some interference between these stray beams which are all at different angles to the main beam and also have different OPDs depending on their paths through the wedges.

The wedge angle in the beamsplitter (and in the compensator plate) is 34 arc min leading to a deviation of the secondary reflection of 56 arc min (the beamsplitter is at a 45° angle). At this radius in the predicted point spread function, and integrating over a small area to allow for the finite size of the fiber, the intensity is estimated to be 0.07% of the input intensity. The total intensity is found by multiplying the appropriate number of times by the beamsplitter reflection coefficient (65%) and the antireflection coating reflection coefficient (0.25%). For two input beams, the total stray light is then approximately 0.13% of the total input light.

Stray light from the rooftop facet (where the surfaces meet) were removed by an aperture at the input, larger than the exit pupil, but sufficiently small to prevent input light from falling on the facet. This entrance aperture also prevented the constructively interfered light reflected by the nuller from returning to the input fiber. This light could potentially cause instability of the laser source. As a further precaution, the input fiber end was polished at an angle to prevent any returned light from reflecting back into the nuller.

Reflections from the exit fiber were minimized by tilting the fiber end slightly to reflect light onto the back of the exit mask. When nulling, these reflections are in any case very small.

Table 1: Constraints on the optical properties of two beams combined to obtain a null depth of 1 part in 10^7. The conditions are approximations based on a deep null and small deviations from perfect matching.

	Optical property	Parameter	Condition	Individual requirements for a 10^{-7} null at 633 nm
1	Intensity matching	Intensity difference Δ	$\Delta = 4\sqrt{N}$	0.13%
2	Strehl ratio matching	Strehl ratio variation σ	$\sigma = 2\sqrt{N}$	0.063%
3	Stray light	Stray light I_{Stray}/I_{Total}	$I_{Stray}/I_{Total} = 4N$	0.00004%
4	Phase matching	Phase difference θ	$\theta = 2\sqrt{N}$	0.00063 radian 0.4 nm
5	Wavefront matching	RMS wavefront difference ϕ	$\phi = 2\sqrt{N}$	0.00063 radian rms 0.4 nm rms
6	Wavefront tilt	Waves across pupil n	$n = 4\sqrt{3N}$	0.0022 waves
7	Shear	Pupil shear h Pupil diameter d_0	$h/d_0 = \sqrt{N}/1.22$	0.026%
8	Polarization matching	Polarization rotation ω	$\omega = 2\sqrt{N}$	0.00063 radian 2.2 arc min
9	Polarization matching	S-P delay difference δ	$\delta = 4\sqrt{N}$	0.0013 radian 0.0002 waves
10	Dispersion	Optical path difference	$(n_1 - n_2)\,l/\lambda = 4\sqrt{N}$	Monochromatic- no dispersion

Stray light from dust that had settled on the mirrors could be seen in the nuller, but this seemed not to affect performance significantly.

Referring to Table 1, null depth contributions from dispersion, parameter 10, were nominally zero since a monochromatic source was used. In fact, the nuller was set up using a broadband light source to establish zero OPD in the nuller for red light of approximately 10% bandwidth. This ensured that any residual laser bandwidth or wavelength drifting would have minimal effect.

We eliminated or minimized null depth contributions from polarization parameters numbered 8 and 9 by using polarizers to transmit only s polarization (considered at the beamsplitter) through the nuller. Polarization control was used at the input to the illuminating fiber where a fiber optic polarization controller was used and at the output stage, prior to the lens focusing down on to the receiving fiber. To maximize the throughput we did not use a polarizer at the laser output but relied on the laser's approximately 100:1 extinction ratio. To clean up the polarization before detection we also employed an output polymer film polarizer before the final focusing lens with an extinction ratio of 500 to 1. These precautions resulted in very high extinction ratios but there was some drifting of polarization during the running of the experiment caused either by polarization angle drift in the HeNe laser or in the fiber coupling into the experiment.

Shear, parameter 7, was eliminated by using a single aperture at the output pupil rather than two separate input apertures. Parameter 6, wavefront tilt, was minimized during initial alignment and by varying it experimentally during nulling. Similarly parameter 4, phase or optical path difference, was varied during the experiments. Parameters 2 and 5, wavefront rms and Strehl ratio, were combined by use of a single mode fiber coupled output: the fiber efficiently couples only a near-Gaussian mode thus selecting principally the lowest spatial frequency modes present in the aperture. This effectively transforms wavefront differences between the two beams into intensity differences. Therefore, by carefully controlling and optimizing the intensity balance of the interferometer arms, we could achieve deep nulls.

To minimize dynamic wavefront errors introduced by atmospheric turbulence, the nuller itself was enclosed in a plexiglass box, while the laser, fiber polarization control system and detectors were located outside the box. To reduce

effects of vibration and noise, and to cut down ambient light, the box sides and top were insulated using foam material. The nuller itself was built on a 2" breadboard stiffened by massive support structures. In turn this breadboard was placed on a 4" optical table and separated from it by a number of vibration absorbing Sorbothane® pucks. This optical table was placed on a larger table supported on vibration damping legs and mounted on a pier attached to bedrock below the building. All these precautions reduced ambient vibrations somewhat, but even so, nulling experiments were generally most successful if conducted late on Friday evenings when the laboratory was relatively quiet. No special precautions were taken when constructing the nuller to reduce thermal effects, and thermal drifting was usually evident. The laboratory containing the nuller was air conditioned, but the fans were turned off when nulling in order to reduce vibration.

Static wavefront quality was dominated by the rooftop prism quality and was ~$\lambda/4$ peak to valley across the full 25 mm aperture, thus far exceeding the requirement of 0.4 nm rms. We selected sub-apertures of the prisms and further cleaned up the wavefront using the fiber output. The output lens and aperture which fed the fiber produced an Airy disc at the focal plane with a diameter of 46 μm at the first dark ring. In contrast the fiber mode field diameter was 4.5 μm, so that it samples only the very core of the point spread function, and effectively is sensitive to very low spatial frequency components of the input field. Such an arrangement is of course very wasteful of light but could be improved upon considerably by using better quality optics to achieve better initial wavefront quality.

8. NULLING EXPERIMENT

The detector was a silicon PIN diode detector attached to a self-ranging power meter. The detector is specified to be linear to ±0.5% over more than 8 orders of magnitude, and the power meter accurate to ±0.1%. Coupling to the detector was via a fiber optic which could be connected to the alternative photon counting module when required for white light experiments. The laser was a HeNe producing 35 mW of which approximately 18 mW was coupled into the input fiber. The fiber was a single mode non-polarization preserving type, wound onto a fiber polarization controller. The output fiber was a similar type. There were significant other power losses in the experiment: the beam expanded to a diameter of ~22 mm at the input lens, of which area only two circles of roughly 5 mm diameter would be used. Taking into account the losses at the exit fiber, the expected throughput was less than 0.04%, and we measured values of several μW, which confirmed this. Near the null, the optical power to be measured would therefore be expected to be tens of nanowatts. The detector baseline could be verified during nulling experiments by closing both shutters. The baseline was normally less than 1 nW, several times lower than our best null. The power meter output was output to a GPIB bus and monitored by graphical software running on a PC. Later the data would be analyzed using a spreadsheet.

The nulling experiment was set up in stages. Initially the system was aligned using the laser and the rooftop mirrors were aligned to point the beams onto the exit fiber. The output and input apertures were then positioned and the input fiber beam visually centered over the input aperture. Then the nuller was run, a null was found and some initial tuning of the null would be done. Then the nuller would be connected to the white light source and the photon counting detector. The white light null would be sought using the piezo-piston fold mirror (see Figure 2) which was attached to a picomotor and a piezoelectric pusher. Once the white light null was found it would be tuned by adjusting the angle of the compensator plate. There are a number of positions of the compensator plate and the piezo-piston fold mirror which result in good nulls (but one of them is best), and by tuning through them, we established an optimum position of the compensator plate. Having found the white light null, the position would remain good enough for laser nulling for several days, so long as no large adjustments were made.

Having completed this initial adjustment of OPD, we adjusted the input fiber to obtain a balance of the power in the two arms. This was done by tilting the input fiber about its tip using a gimbal stage and measuring the power in the two arms sequentially by closing the shutters alternately. After progressively adjusting, we were able to obtain intensity balances of the 0.1% order required for high contrast nulling.

This completed, we reconnected the laser source and detector. Nulling proceeded by a series of tuning trials in which we alternately searched the point spread functions of the two arms for an optimum null. Each arm could be adjusted in one axis and so we progressively adjusted the tilt of each rooftop mirror while tuning the OPD for null. Nulls were usually quite unsteady and strongly affected by laboratory noise and vibration. The horizontal arm of the nuller was particularly

sensitive to this. In addition there was continual drifting of the zero of OPD caused presumably by small temperature changes in the laboratory. The experiments were performed in near-darkness because room light and light from indicators on instrumentation in the room leaking into the exit fiber could cause significant offsets of the detector baseline and therefore apparently degrade the null.

Using variously sized circular apertures between 6.0 and 4.7 mm diameter at the output we found that the intensity of the light at the detector varied roughly as aperture radius to the fourth power, as expected, but below a certain size there was little effect on maximum null depth suggesting that wavefront quality was not the driving factor. Observation of the beams in the nuller showed faint fringes across the beam, probably produced by the secondary reflections in the wedges. As noted above, secondary focal spots would be present in the focal plane which will introduce some stray light into the exit fiber.

9. RESULTS

Figure 4 shows data from an experiment which achieved transient nulls better than 1 part in 10^6. At about the 6 seconds mark, both shutters are closed so that the baseline power reading can be made; it is approximately 5.9 pW. Between about 3 and 11 seconds into the run we can see the two shutters opened alternately exposing the two interferometer arms. After 11 seconds, both shutters are opened and the OPD is tuned to the constructive fringe. Peak power is approximately 15.2 μW. After 20 seconds the OPD is tuned to the destructive fringe and various fine adjustments are made to the nuller alignments and OPD settings to attempt a deep null. Finally after 43 seconds the nuller is retuned to the constructive fringe.

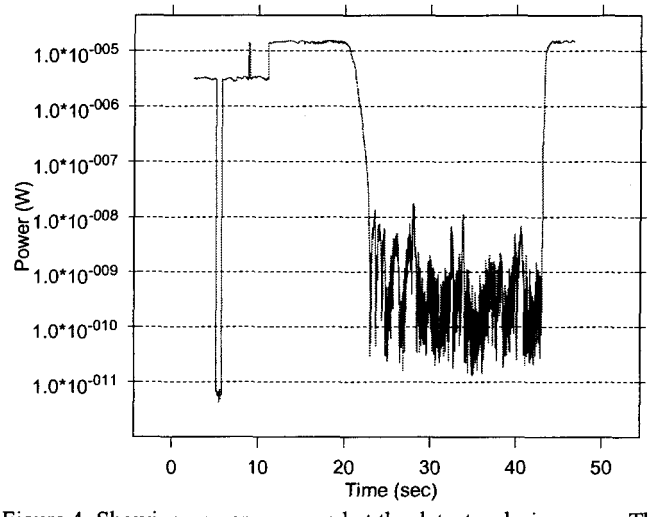

Figure 4: Showing power measured at the detector during a run. The dip at approximately 6 secs is a measurement of the dark baseline with mean measured power level of approximately 5.9 pW. Between 12 and 20 seconds into the run we see the top of the constructive fringe with power levels of 15 μW. During nulling, the power drops occasionally to minimum values of 12.6 pW from more typical values of 100 pW.

Figure 4 shows the same data plotted to show the null depth, the best null achieved here is 0.83 10^{-6}. A number of other datasets were acquired with transient nulls of better than 10^{-6} but these data were relatively rare, and in the best longer periods of performance (a second or so) , the mean null depth could be held to around 3 to 5 10^{-6}. The best null measured was a transient null of 0.744 10^{-6}. Based on the ambient light level with the shutters closed, the best null achievable would be 0.39 10^{-6}, so the measured best null is within a factor of two of this.

10. LIMITATIONS TO NULL DEPTH

Earlier experiments using a 5 mW HeNe laser had achieved transient null depths of 2.04 10^{-6} which were baseline noise limited. The baseline noise level with that laser was 1.53 pW with a standard deviation of 1.10 pW. A few very deep nulls were recorded which had power levels of less than 1 pW, so these nulls occurred when the power was below the mean noise floor. To overcome this problem, we used the higher power laser with which we able to more consistently achieve deep nulls, and also extended the best transients below the 10^{-6} level.

The stability of the nulls with either laser was limited, but using automatic path length control systems described elsewhere[10] we achieved a few times better stability at least for 10^{-5} level nulls. Also, our apparatus was not particularly stable, being built largely from off the shelf components, the large numbers of stages and adjusters adding many degrees of freedom for motion of the optics. We were only partially successful in eliminating background vibration as was

apparent from the improved results obtained during evening experiments compared with nulling attempts at other times during the day.

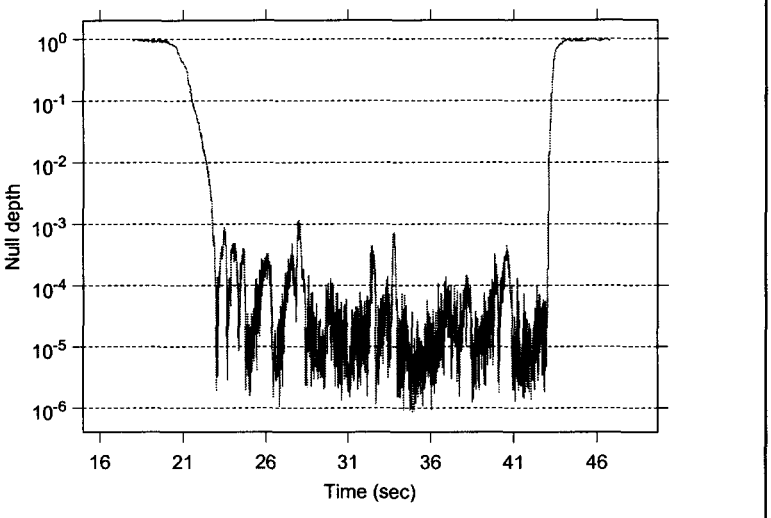

Figure 5: Data from Figure 4 plotted as null depth over time.

Concerning null depth, it was observed that the polarization of the laser beam was drifting during the experiments, so we introduced a second polarizer to raise the extinction ratio, but without effect. We also observed that null depth seemed insensitive to aperture size (between 4.7 and 6 mm), suggesting that wavefront quality and stray light might be only weakly linked to the final performance. In order to achieve nulls as deep as those recorded here, the system must meet stringent requirements and we concluded that to achieve deeper nulls and more stability, a number of improvements would need to be made to the system as a whole, and an important improvement would be to increase the wedge angle of the beamsplitter. This change would of course limit broadband performance. In fact the performance of the nuller approaches the theoretical best for this layout if we assume the stray light level measured with the shutters closed is the same as the stray light level during the experiments and we add the expected stray light contribution from the beamsplitter wedging, we would expect the best nulls to be at the 0.85 10^{-6} level.

11. CONCLUSION

At the Jet Propulsion Laboratory, we are now building nullers based on a modified Mach-Zehnder (MMZ) layout[12]. These designs offer some advantages with fewer mirrors and components, and two-dimensional rather than three-dimensional layout. The degree of symmetry is higher since no compensator plate is required, but beamsplitters must still be wedged, which produces some small asymmetries. These new designs are currently being used for broadband mid-IR nulling, with a pair of nullers destined for the Keck telescopes nearing completion. In the laboratory, narrowband nulls of 1.25 10^{-4} have already been achieved with this system.

The work described herein was carried out at the Jet Propulsion Laboratory, California Institute of Technology, under contract with the National Aeronautics and Space Administration.

REFERENCES

1. Hinz, P. M., Angel, J. R. P., Hoffmann, W. F., McCarthy, D.W, McGuire, P. C., Cheselka, M., Hora, J. L., & Woolf, N. J. Imaging circumstellar environments with a nulling interferometer, Nature 395, 251-253 (1998).
2. Terrestial Planet Finder (TPF) 1999, edited by C. A. Beichman, N. J. Woolf, & C. A. Lindensmith (Jet Propulsion Laboratory: Pasadena, CA), JPL Publication 99-3.
3. Colavita, M.M., Boden, A.F., Crawford, S.L., Meinel, A.B., Shao, M., Swanson, P.N., van Belle, G.T., Vasisht, G., Walker, J.M., Wallace, J.K. & Wizinowich, P.L., The Keck Interferometer, Proc. SPIE 3350, 776-784 (1998).
4. Leger, A., Mariotti, J.-M., Menneson, B., Ollivier, M., Puget, J.L., Rouan, D. & Schneider, J. Could we search for primitive life on extrasolar planets in the near future?: The DARWIN project, Icarus 123, 249-255 (1996).
5. K. Wallace, G. Hardy & E. Serabyn, "Deep and Stable Interferometric Nulling of Broadband Light with Implications for Observing Planets around Nearby Stars," Nature 406, 700–702, 2000.

6. Diner, D. J., IBIS: an interferometer-based imaging system for detecting extrasolar planets with a next generation space telescope, in The Next Generation Space Telescope, (eds. Bely, P.Y., Burrows, C.J. & Illingworth, G.D.), 133-141 (Space Telescope Science Institute, Baltimore,1990).
7. Shao, M., Direct IR interferometric detection of extra solar planets, in The Next Generation Space Telescope, (eds. Bely, P.Y., Burrows, C.J. & Illingworth, G.D.), 160-168 (Space Telescope Science Institute, Baltimore,1990).
8. Angel, J.R.P., Use of a 16 m telescope to detect earthlike planets, in The Next Generation Space Telescope, (eds. Bely, P.Y., Burrows, C.J. & Illingworth, G.D.), 81-94 (Space Telescope Science Institute, Baltimore,1990).
9. R.M. Morgan, J. Burge, & N. Woolf, "Nulling interferometric beam combiner using dielectric plates: experimental results in the visible broadband,'' Interferometry in Optical Astronomy, Proc. SPIE 4006, *340–348*, 2000.
10. E. Serabyn, S.R. Martin & G.J. Hardy, "Progress Toward Space-based Nulling Interferometry: Comparison of Null Stabilization Approaches,'' Proc. 2001 IEEE Aerospace Conference, 2001.
11. E. Serabyn, "Nulling Interferometry: Symmetry Requirements and Experimental Results,'' Interferometry in Optical Astronomy, Proc. SPIE 4006, 328–339, 2000.
12. E. Serabyn & M. M. Colavita, "Fully Symmetric Nulling Beam Combiners,'' Appl. Opt. 40, 1668–1671, 2001.